Abstract

Controlling Morphological Development during Additive Manufacturing: A Route to the Mapping of Properties [†]

Daniel Silva [1], João Pinheiro [1], Saba Abdulghani [1] , Christina S Kamma-Lorger [2], Eduardo Solano [2] , Juan Carlos Martinez [2], Paula Pascoal-Faria [1] , Artur Mateus [1] and Geoffrey R Mitchell [1,*]

[1] Centre for Rapid and Sustainable Product Development, Polytechnic of Leiria, 2430-080 Marinha Grande, Portugal; daniel.p.silva@ipleirira.pt (D.S.); joao.pinheiro@ipleiria.ptm (J.P.); saba.abdulghani@nms.unl.pt (S.A.); paula.faria@ipleiria.pt (P.P.-F.); artur.mateus@ipleiria.pt (A.M.)

[2] NCD-SWEET Beamline, Alba Synchrotron Light Source, Cerdanyola del Vallès, 08290 Barcelona, Spain; ckamma@ansto.gov.au (C.S.K.-L.); esolano@cells.es (E.S.); guilmar@cells.es (J.C.M.)

* Correspondence: geoffrey.mitchell@ipleiria.pt; Tel.: +351-962-426-925

[†] Presented at the Materiais 2022, Marinha Grande, Portugal, 10–13 April 2022.

Direct digital manufacturing (DDM) is a family of technologies which enables products to be manufactured directly from a digital definition without the use of specialized tooling or molds [1]. Fused deposition modelling and stereolithography are probably the most common and widely used of these transformation technologies. These have developed out of techniques to rapidly produce prototypes of products from design or marketing ideas. Since their development, the range of materials used has widened to include materials from which actual products can be produced, and from which all of the properties required can be exhibited. Although there have been many advances in 3D printing technology, most of the focus has been on producing in hi-fidelity shapes from a digital definition. Little attention has been placed on developing technology to focus on other aspects beyond the simple form of a product. This work seeks to readdress this area.

Here, we focus on the use of 3D printing to produce plastic parts. Essentially, a thin strand of molten polymer is extruded onto a moving build platform in a defined manner to build up a structure layer by layer. As with any polymer processing technology, the process conditions will influence the polymer morphology and structure upon cooling which, in turn, will impact the properties. As part of a major project to fully understand all aspects of 3D printing, we performed small-angle X-ray scattering (SAXS) experiments on parts prepared in this manner on the NCD-SWEET beamline at the ALBA Synchrotron Light Source in Barcelona, Spain. We designed and built a 3D printer which can be mounted on the ALBA NCD-SWEET beamline so we can follow the structural development in real time [2]. We will show examples of how the printing parameters affect the structure and morphology, we will describe the experiments which have been performed, and we will discuss the type of information we have been able to extract. We will show how the results we obtain can be used to optimize 3D printing technology and the materials used, and how this approach can be used to produce patterns or variations in properties. In short, we will show how we can print properties, and not just shape.

This work is focused on the 3D printing of low-density polyethylene (LDPE). The material used was Respol LDPE, Alcudia 1970C, with a melt flow index of 7.5 g/10 mins equating to a molecular weight of $\sim 7 \times 10^4$ Daltons. [3]. Differential scanning calorimetry measurements showed that the onset of crystallization in LDPE happens at 94.2 °C with a maximum rate of crystallization observed at 90.2 °C. These measurements relate to the quiescent melt and the values may be modified by the flow processes inherent in extrusion.

We performed in situ time-resolving small-angle X-ray scattering measurements using the NCD-SWEET beamline at the ALBA Synchrotron Light Source in Barcelona. The beamline contains facilities for measuring both SAXS and WAXS simultaneously. SAXS patterns were taken in a Q-range from 0.0017 Å^{-1} to 0.125 Å^{-1} and the WAXS patterns from 1.0 Å^{-1} to 3 Å^{-1}. The SAXS Detector was a DECTRIS Pilatus3S 1M system, which is a hybrid single-photon counting system. The Pilatus system is built up of a number of silicon sensors and, as a consequence, a small portion of the detector is not sensitive (~7%), appearing as black stripes in the recorded intensity images. This detector has a pixel size of 172 × 172 micrometers with a dynamic range of 0–1,048,576. To stop the saturation of the detector by the zero-angle X-ray beam, an absorbing beam stop was placed in front of the detector to absorb the transmitted beam. The sample to SAXS detector distance was 6.81 m with an incident X-ray wavelength of 1 Å. The detector orientation and sample to detector distance was calibrated using the well-known standard silver behenate. The WAXS detector was a triple-cooled CCD detector bonded by fiber-optic tapers to the X-ray photon detector surface with a pixel size of 44.27 × 44.27 micrometers (Rayonix LX255 HS). The geometry and the shape of the detector ensured that the direct beam and the SAXS pattern were not blocked by the WAXS detector. The WAXS detector orientation and sample to detector distance were calibrated using Cr_2O_3. For each 2D SAXS pattern, an azimuthal section I(α) was obtained at constant |Q| and as a function of α, where α is the angle between the extrusion axis which is vertical to the beamline and the scattering vector Q. The azimuthal section I(α) was used to evaluate the level of preferred orientation of the chain-folded lamellar crystals using the methodology developed by Mitchell et al. [4–7] and is shown in Equation (1).

$$\langle P_{2n}\rangle_Q = \frac{1}{(4n+1)P_2{}^m} \int_0^{\pi/2} \frac{I(|\underline{Q}|,\alpha)\sin\,\alpha P_2\,(\cos\alpha)\,d\alpha}{I(|\underline{Q}|,\alpha)\sin\alpha\,d\alpha} \tag{1}$$

The orientation parameter $<P_2>$ is the first component of an even series which describes the orientation distribution function of the normal to the lamellar crystals. If $<P_2>$ = 0, the distribution is isotropic; if $<P_2>$ = 1, the crystals are arranged with the same perfect preferred orientation.

The physical constraints of the beamline and the proximity of the delicate components place considerable restrictions on the 3D printer stage. As a consequence, we designed and constructed a pellet-fed extruder-based 3D printer specifically for these experiments, and Figure 1 shows the 3D printer mounted on the NCD-SWEET beamline. The extruder-based printer was largely based on the bio-extruder system also developed at CDRSP [8], with the flat translational build platform replaced with a rotational build surface. A rotational build platform was chosen so as to provide the possibility of higher write speeds if required, and to maintain a clean build surface. The complete system could be controlled remotely, including extruder temperature, extrusion rate, and the write velocity (relative speed of print head to the build platform). The extruder die was a needle with an internal diameter of 300 μm.

The extruded filament is in a molten state as it emerges from the extruder; the temperature of the filaments drops continuously until it reaches the crystallization temperature, the material transforms to a solid, and the printed shape is preserved. The temperature profiles of the surroundings to the extruded filament are constant, and so we can see the filament in a quasi-steady state in which the evolution of the structure and morphology of the extruded material with time can be sampled by arranging the incident X-ray beam to move to different positions along the filament from close to the extruder die to near to the build platform. This process can be automated on the beamline and, for a typical experiment, we moved in 20 steps of 0.1 mm with a 1-second data-collection period. Figure 2 shows SAXS scattering patterns recorded for filaments prepared with the same extruder temperature and extrusion rate but with different write speeds at the point in the filament just before the build platform. The SAXS patterns are typical for a semi-crystalline polymer. Figure 2A

shows a more or less isotropic ring indicating an isotropic distribution of lamellar crystals. Figure 2C shows a highly anisotropic distribution of scattering, indicating a high level of lamellar crystals with a common orientation. Figure 2B is recorded for an intermediate write speed and contains a mixture of both isotropic scattering and highly anisotropic scattering. Figure 3 shows the wide-angle X-ray scattering recorded at the same time as for Figure 2C. The pattern shows the intense peaks for polyethylene, namely the (110) and (200) peaks. These crystalline peaks are more intense at certain points of the azimthual range, indicating the development of an anisotropic morphology. We note that the anisotropy revealed in the WAXS pattern is less marked than that observed in the SAXS pattern. This underlines the challenge in using WAXS patterns to evaluate preferred orientation in semi-crystalline polymers. It is common to observe for LDPE that the chain-folded lamellar crystals adopt a twisted arrangement, which means that that the evaluation of the preferred orientation of the lamellar crystals cannot be made simply from the WAXS patterns.
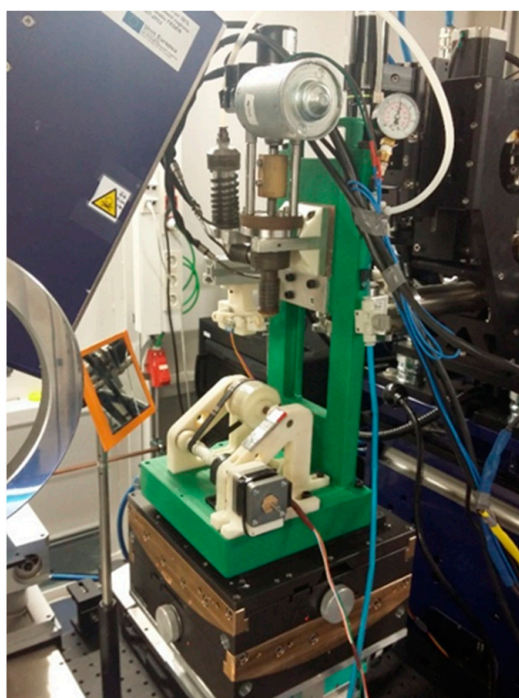

Figure 1. A photograph of the 3D printer developed for these experiments mounted on the NCD-SWEET beamline at ALBA; the incident beam enters from the right, and the front face of the WAXS detector can be seen on the left-hand side.
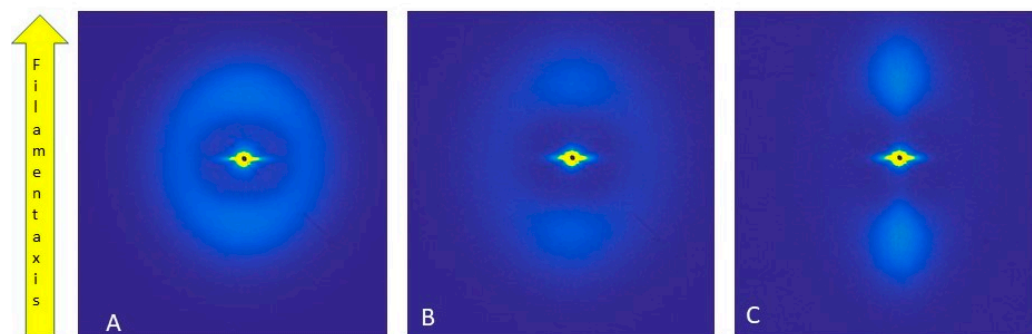

Figure 2. SAXS scattering patterns from the last point of each scan of the filament for LDPE with an extrusion temperature of 170 °C at a constant extrusion rate with different write speeds: (**A**) slow, (**B**) medium, and (**C**) fast.
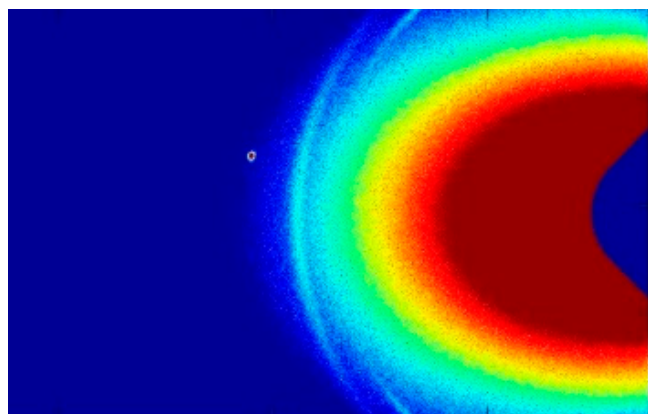
Figure 3. The WAXS recorded at the same time as Figure 2C. The scattering angle increases from left to right. Only the lower half of the angular range is shown in this figure corresponding to a Q range of 1 to 2 A^{-1}.

We have shown that the printing parameters used in a 3D printer can be used to generate printed filaments with differing morphologies and with different levels of preferred orientation of the lamellar crystals, ranging from an isotropic distribution to a highly anisotropic distribution. These differing morphologies will impart different mechanical properties to the material. If we are able to change the print parameters during the printing process, we will have a methodology for printing parts of the object with different properties and generating gradients of properties with more complex patterns. The resolution of these changes in properties will depend on how quickly the parameters can be changed and how long it will take for the changes to take effect. The changes in extrusion rate and write speed are more or less instantaneous, as they are read and set from the g-code file. Changes to the extruder temperature will naturally have a time delay, although it may be possible to reduce this by design to a tolerable level.

We have shown that the normal parameters in a 3D printer can be used to control the structure and morphology of the printed material in the case of a semi-crystalline polymer with an attendant change in the physical properties. This introduces the possibility of printing properties rather than simply producing shapes with uniform properties. This development opens up possibilities for the novel design of products and greatly extends the advantages of 3D printing within the scope of direct digital manufacturing.

Institutional Review Board Statement: Not Applicable.

Informed Consent Statement: Not Applicable.

Data Availability Statement: The data obtained using the facilities of the ALBA Synchrotron Light Source are subject to the Generic data management policy at ALBA CELLS as can be accessed at Microsoft Word—Data_policy_Alba_v1.2_2017.doc (cells.es). The experimental data identifiers are available from the corresponding author after the end of the embargo period.

Conflicts of Interest: The authors declare no conflict of interest.

References

1. Gibson, I.; Rosen, D.; Stucker, B. *Additive Manufacturing Technologies 3D Printing, Rapid Prototyping, and Direct Digital Manufacturing*; Springer: Berlin/Heidelberg, Germany, 2015; ISBN 978-1-4939-2113-3.
2. Da Silva, D.P.; Pinheiro, J.; Abdulghani, S.; Kamma Lorger, C.; Martinez, J.C.; Solano, E.; Mateus, A.; Pascoal-Faria, P.; Mitchell, G.R. Changing the Paradigm-Controlling Polymer Morphology during 3D Printing Defines Properties. *Polymers* **2022**, *14*, 1638. [CrossRef] [PubMed]
3. Azmi, A.; Sata, S.A.; Rohman, F.S.; Aziz, N. Melt flow index of low-density polyethylene determination based on molecular weight and branching properties. In *Journal of Physics: Conference Series*; IOP Publishing: London, UK, 2019. [CrossRef]
4. Lovell, R.; Mitchell, R.G.; Cryst, A. Molecular orientation distribution derived from an arbitrary reflection. *Acta Crystallogr. Sect. A Cryst. Phys. Diffr. Theor. Gen. Crystallogr.* **1981**, *37*, 135–137. [CrossRef]
5. Mitchell, G.R.; Saengsuwan, S.; Bualek-Limcharoen, S. Evaluation of preferred orientation in multi-component polymer systems using X-ray scattering procedures. In *Scattering Methods and the Properties of Polymer Materials*; Springer: Berlin/Heidelberg, Germany, 2005; pp. 149–158.
6. Mohan, S.D.; Olley, R.H.; Vaughan, A.S.; Mitchell, G.R. Evaluating Scales of Structure in Polymers. In *Controlling the Morphology of Polymers: Multiple Scales of Structure and Processing*; Mitchell, E.G., Tojeira, A., Eds.; Springer: Berlin/Heidelberg, Germany, 2016; ISBN 978-3-319-39320-9.
7. Pinheiro, J.; Abdulghani, S.; Pascoal-Faria, P.; Sousa, D.; Carreira, P.; Viana, T.; Kamma-Lorger, C.S.; Mitchell, G.R. 2019 AIP Conference Proceedings 2116. In Proceedings of the International Conference on Numerical Analysis and Applied Mathematics, Rhodes, Greece, 13–18 September 2018. [CrossRef]
8. Almeida, H.A.; Bártolo, P.J.; Mota, C.M.; Mateus, A. E Equipamento de Fabrico Rápido por Bioextrusão. Portuguese Patent 104247, 2010.